 

*METHODOLOGICAL NOTES*

PACS number: 42.65.Re

# Nonlinear dynamics of high-power ultrashort laser pulses: exaflop computations on a laboratory computer station and subcycle light bullets

A A Voronin, A M Zheltikov

DOI: 10.3367/UFNe.2016.02.037700

## Contents


| | | |
|---|---|---|
| 1. | Introduction | 869 |
| 2. | Physical model | 870 |
| 3. | Numerical methods | 871 |
| 4. | Exaflop computations on a laboratory computer station | 872 |
| 5. | Dynamics of multiple filamentation | 872 |
| 6. | Self-compression of high-peak-power light pulses | 874 |
| 7. | Subcycle light bullets | 874 |
| 8. | Conclusion | 876 |
| | References | 876 |


**Abstract.** **The propagation of high-power ultrashort light pulses involves intricate nonlinear spatio-temporal dynamics where various spectral–temporal field transformation effects are strongly coupled to the beam dynamics, which, in turn, varies from the leading to the trailing edge of the pulse. Analysis of this nonlinear dynamics, accompanied by spatial instabilities, beam breakup into multiple filaments, and unique phenomena leading to the generation of extremely short optical field waveforms, is equivalent in its computational complexity to a simulation of the time evolution of a few billion-dimensional physical system. Such an analysis requires exaflops of computational operations and is usually performed on high-performance supercomputers. Here, we present methods of physical modeling and numerical analysis that allow problems of this class to be solved on a laboratory computer boosted by a cluster of graphic accelerators. Exaflop computations performed with the application of these methods reveal new unique phenomena in the spatio-temporal dynamics of high-power ultrashort laser pulses. We demonstrate that unprecedentedly short light bullets can be generated as a part of that dynamics, providing optical field localization in both space and time through a delicate balance between dispersion and nonlinearity with simultaneous suppression of diffraction-induced beam divergence due to the joint effect of Kerr and ionization nonlinearities.**

**A A Voronin** Lomonosov Moscow State University, Faculty of Physics, Leninskie gory 1, str. 2, 119991 Moscow, Russian Federation; Lomonosov Moscow State University, International Laser Center, Leninskie gory 1, str. 62, 119991 Moscow, Russian Federation; International Center for Quantum Optics and Quantum Technologies (Russian Quantum Center), ul. Novaya 100a, 143025 Skolkovo, Moscow, Russian Federation

**A M Zheltikov** Lomonosov Moscow State University, Faculty of Physics, Leninskie gory 1, str. 2, 119991 Moscow, Russian Federation; Lomonosov Moscow State University, International Laser Center, Leninskie gory 1, str. 62, 119991 Moscow, Russian Federation; International Center for Quantum Optics and Quantum Technologies (Russian Quantum Center), ul. Novaya 100a, 143025 Skolkovo, Moscow, Russian Federation; Texas A&M University, Department of Physics and Astronomy, College Station, Texas 77843, USA; National Research Centre 'Kurchatov Institute', pl. Kurchatova 1, 123182 Moscow, Russian Federation

E-mail: zheltikov@physics.msu.ru

Received 24 January 2016
*Uspekhi Fizicheskikh Nauk* **186** (9) 957 – 966 (2016)
DOI: 10.3367/UFNr.2016.02.037700
Translated by A M Zheltikov; edited by A Radzig

**Keywords:** ultrashort laser pulses, ultrafast nonlinear optics, laser-induced filamentation

## 1. Introduction

Rapid progress in laser technologies is giving rise to a new generation of high-power sources of ultrashort pulses of electromagnetic radiation capable of delivering ultrahigh-intensity, ultrahigh-peak-power laser pulses at a high repetition rate within a broad spectral range [1, 2]. Propagation of such pulses through a medium is accompanied by a complex nonlinear evolution [3–5], where various spectral–temporal field transformations are strongly coupled to spatial beam dynamics, which, in turn, is nonuniform within the laser pulse (Fig. 1a). Such regimes of pulse propagation are of special interest in the context of long-distance transmission of high-power ultrashort pulses through the atmosphere [6, 7], efficient white-light supercontinuum generation [8–13], and temporal compression of high-power ultrashort pulses [14–16] in the laser filamentation regime. Lasing in laser-induced

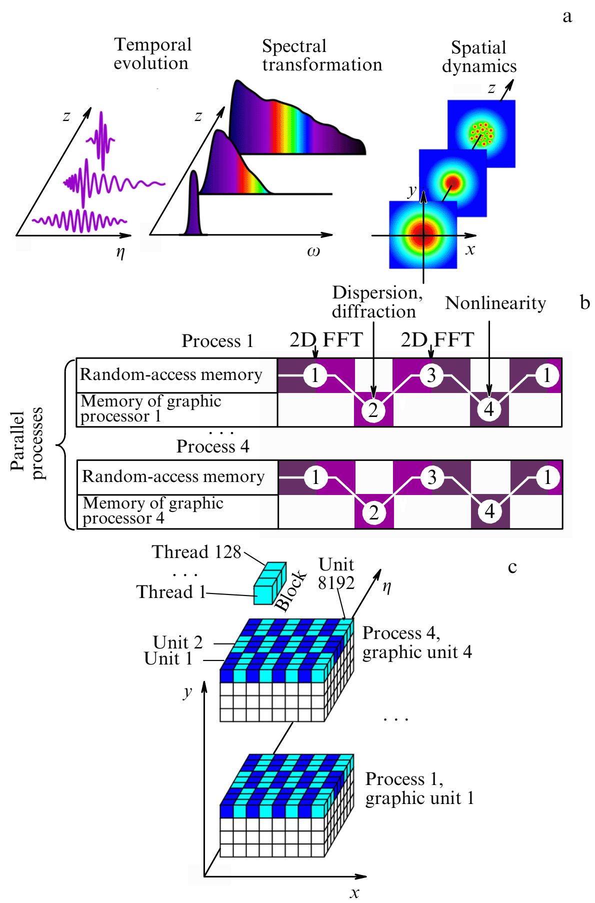


**Figure 1.** (Color online). (a) Spatio-temporal dynamics of a high-peak-power ultrashort light pulse in a $(3+1)$-dimensional problem in spatial $x$, $y$, and $z$ coordinates and time $\eta$ in the retarded frame of reference running with the pulse: (left) temporal evolution of the pulse, (center) spectral transformation and supercontinuum generation, and (right) spatial dynamics involving modulation instability of the beam leading to the loss of axial symmetry. (b) Diagram of computations at each step of the numerical algorithm. The number of parallel MPI processes is defined by the number of graphic processors $M$ (for the developed laboratory computer station, $M=4$). (c) Parallel computations determining the nonlinear operator, performed by graphic processors on an $xy\eta$ grid including $512\times512\times2048$ nodes. Grid node layers in the $x\eta$ plane within which each of the graphic processors performs parallel computations are shown in color.

filaments [17] offers unique opportunities for a highly sensitive remote sensing of the atmosphere [18, 19].

When the peak power of an ultrashort pulse is much higher than the self-focusing threshold, a light beam becomes unstable [20] with respect to a breakup to multiple filaments (Fig. 1a). Since such beam instabilities are seeded by random intensity fluctuations across a laser beam or optical inhomogeneities of a medium, a laser beam undergoing multiple filamentation usually loses its axial symmetry. In each of the filaments arising as a part of this process, diffraction is suppressed due to the joint action of nonlinear polarization induced in the medium and the radial profile of electron density [3, 4, 21]. Within a limited parameter space, as recent studies have shown [22], high-power single-cycle and subcycle optical pulses can be generated in laser filaments, giving rise to ultrashort bursts of electromagnetic fields, whose duration is less than a field cycle. The correct analysis of this intriguing regime of pulse evolution is not possible in the ordinary slowly varying envelope approximation (SVEA) and requires the inclusion of all the relevant non-SVEA effects in the nonlinear spatio-temporal dynamics of high-power ultrashort light pulses.

The diversity of physical phenomena involved in this regime of nonlinear spatio-temporal field evolution and the related physical scenarios that may lead to the formation of single-cycle and subcycle pulses can only be understood in the framework of a full model of spatio-temporal field dynamics, including all the relevant non-SVEA effects. Since single-cycle and subcycle pulses need to be adequately described, numerical analysis has to be performed with a high resolution in spatial and temporal coordinates within the entire pathway of nonlinear interaction, which is often very long in the regime of laser filamentation. Such an analysis is equivalent in its computational complexity to a modeling of the temporal evolution of a physical system possessing a few billion degrees of freedom. Its implementation requires exaflop computations and is usually performed with the aid of supercomputers.

Here, we present methods of physical modeling and numerical analysis that allow problems of this class to be solved on a laboratory computer with a cluster of graphic processing units (GPUs). Exaflop computations performed with the use of these strategies reveal new unique phenomena of the spatio-temporal dynamics of superpower ultrashort light pulses, including the generation of single-cycle and subcycle field waveforms. In special regimes of nonlinear dynamics, such field waveforms are shown to evolve into multiple light bullets.

## 2. Physical model

The spatio-temporal dynamics of high-power ultrashort pulses is analyzed using the generalized nonlinear Schrödinger equation (GNSE) for the complex field amplitude involving ultrafast field-induced ionization processes [3–5, 23, 24]:

$$
\begin{aligned}
\frac{\partial}{\partial z}A(\omega,x,y,z) &= \left[\frac{\mathrm{i}c}{2\omega_0 n_0}\Delta_\perp + \mathrm{i}\tilde{D}(\omega)\right]A(\omega,x,y,z)\\
&+\tilde{F}\bigg\{\mathrm{i}\,\frac{\omega_0\tilde{T}}{c}\bigg[n_2(1-f_\mathrm{R})\,I(\eta,x,y,z)\\
&+\sum_{q=2}^{4}n_{2q}I^{2q}(\eta,x,y,z)\bigg]A(\eta,x,y,z)\\
&+n_2 f_\mathrm{R}\int_{-\infty}^{\infty}R(\eta-\eta')\,I(\eta',x,y,z)\,\mathrm{d}\eta'\,A(\eta,x,y,z)\\
&+\sum_{s=2}^{5}\frac{\chi^{(2s-1)}}{2^s c^{s-1}\varepsilon_0^{s-1}}A^{2s-1}(\eta,x,y,z)\\
&-\left(\frac{\mathrm{i}\omega_0}{2cn_0\rho_\mathrm{c}\tilde{T}}\,\rho+\frac{U_\mathrm{i}W(\rho_0-\rho)}{2I}+\frac{\sigma}{2}\,\rho\right)A(\eta,x,y,z)\bigg\}\,. \qquad (1)
\end{aligned}
$$

Here, $A(\eta,x,y,z)$ is the complex field amplitude, $A(\omega,x,y,z)$ is its Fourier transform, $I(\eta,x,y,z)=|A(\eta,x,y,z)|^2$ is the field intensity, $\eta$ is the retarded time, $x$ and $y$ are the transverse coordinates, $z$ is the coordinate along the propagation axis, $\omega$ is the radiation frequency, $\Delta_\perp=\partial^2/\partial x^2+\partial^2/\partial y^2$ is the diffraction operator, $\tilde{D}=k(\omega)-k(\omega_0)-\partial k/\partial\omega|_{\omega_0}(\omega-\omega_0)$ is the dispersion operator, $\omega_0$ is the central frequency of the laser pulse, $k(\omega)=\omega n(\omega)/c$ is the wave number, $n(\omega)$ is the refractive index, $n_0=n(\omega_0)$, $\tilde{F}$ is the Fourier transform operator in the time variable, $\chi^{(3)}$, $\chi^{(5)}$, $\chi^{(7)}$, and $\chi^{(9)}$ are the third-, fifth-, seventh-, and ninth-order nonlinear-optical susceptibilities, $n_2$, $n_4$, $n_6$, and $n_8$ are the Kerr nonlinearity coefficients, $\tilde{T} = 1 + \mathrm{i}\omega_0^{-1}\,\partial/\partial\eta$, $R(\eta)$ is the Raman response function, $f_R$ is the fraction of the Raman (delayed) nonlinearity in the overall nonlinear response of the medium, $\rho$ is the electron density, $U_i = U_0 + U_{osc}$, $U_0$ is the ionization potential, $U_{osc}$ is the ponderomotive energy of field-induced electron oscillations, $W(I)$ is the photoionization rate, $\sigma$ is the avalanche ionization cross section, $\rho_c = \omega_0^2 m_e \varepsilon_0/e^2$ is the critical electron density, $\rho_0$ is the neutral gas density, $m_e$ is the electron mass, $e$ is the electron charge, and $\varepsilon_0$ is the permittivity of a vacuum.

Field evolution equation (1) is solved jointly with the equation for the electron density, which involves field-induced ionization, as well as avalanche ionization and recombination:

$$\frac{\partial\rho}{\partial\eta} = W(I) + \sigma(\omega_0)\,U_i^{-1}\rho I - \frac{\rho}{\tau_r}\,, \tag{2}$$

where $\tau_r$ is the recombination time. The photoionization rate $W$ in equations (1) and (2) is calculated applying the Keldysh formalism [25, 26]. The avalanche ionization cross section $\sigma$ is calculated with the use of the Drude formula $\sigma(\omega) = e^2\tau_c[m_e\varepsilon_0 n_0 c(1+\omega^2\tau_c^2)]^{-1}$, where $\tau_c$ is the characteristic collision time.

The model based on Eqns (1) and (2) comprises all the key physical effects that show up in the evolution of high-power ultrashort pulses in a nonlinear dispersive medium. The spectral representation of the dispersion operator $\tilde{D}$ allows the material dispersion to be described exactly rather than through its polynomial expansion about the central frequency $\omega_0$. An accurate description of material dispersion is of crucial importance for the analysis of a broad class of nonlinear optical processes, including multioctave supercontinuum generation, as well as single-cycle and subcycle pulse generation, where the models based on a series expansion of the frequency dispersion profile in $\omega - \omega_0$ fail. The physical model adopted in our work also includes linear loss and diffraction effects, the field-induced change in the refractive index due to the third-, fifth-, and, whenever necessary, higher-order Kerr type optical nonlinearities, pulse self-steepening, spatio-temporal self-action phenomena, as well as plasma loss, dispersion, scattering, and, finally, defocusing due to an ultrafast ionization of the medium by the laser field.

Field evolution equation (1) is solved by the split-step method. The linear diffraction and dispersion operators in this equation are computed using the Fourier method. The nonlinear part of the field evolution equation, as well as the equation for the electron density dynamics, are solved by the fourth- or fifth-order Runge–Kutta method.

Importantly, the assumption of an axially symmetric beam, which substantially simplifies the solution of equation (1), fails in the regime of multiple filamentation. In this regime, a laser beam tends to break up into multiple filaments due to spatial modulation instabilities arising from random hot spots across the beam, seeded by noise-induced intensity fluctuations and random optical inhomogeneities in the medium. In its fully three-dimensional version, field evolution equation (1), which also involves a time variable and is, hence, often referred to as a $(3+1)$-dimensional model, leads to calculations of high computational complexity.

## 3. Numerical methods

To provide the accuracy sufficient for an adequate description of single-cycle and subcycle pulse generation, the computational grid used in simulations has to have a step in time well within the optical cycle. The overall sizes of the grid, on the other hand, have to be large enough to accommodate the entire laser pulse and all the field components generated at each point in space and time and propagating with fundamentally different group velocities.

For a 1- to 10-cycle optical pulse, depending on the field intensity and beam-focusing geometry, this typically dictates a grid with 1024 to 4096 nodes in the time variable. An accurate modeling of subcycle pulses often requires computational grids with an even larger number of nodes.

Analysis of nonlinear beam dynamics is performed on a two-dimensional grid whose step in transverse coordinates has to be much smaller than the size of individual filaments. The most efficient pulse compression is often confined to a small area near the beam axis. The two-dimensional spatial grid for beam dynamics modeling has to be fine enough to resolve and accurately describe this effect. However, on the other hand, the overall sizes of the grid should be large enough to completely accommodate the spatial field components, which may be generated within a broad range of angles and can undergo focusing by the Kerr lens and diffraction by the transverse electron density profile, increasing this range of angles even further. For peak powers below 100 critical powers of self-focusing, these requirements can usually be satisfied with grids possessing $512 \times 512$ to $1024 \times 1024$ nodes.

The maximum admissible step along the longitudinal coordinate is typically determined from the condition that the nonlinear phase shift not exceed 0.025 rad if the nonlinear operator in equation (1) is computed using the fourth-order Runge–Kutta method, and 0.05 rad if the fifth-order Runge–Kutta method is employed. The overall extension of the grid along the longitudinal coordinate is determined by the integral nonlinear phase shift. To model a typical experiment on multiple filamentation of high-power ultrashort laser pulses, the number of grid steps along the longitudinal coordinate should be on the order of 10,000.

Thus, a $(3+1)$-dimensional analysis of the evolution of a high-power ultrashort laser pulse with a fixed set of parameters in the regime of multiple filamentation typically yields a data array of 10–100 Tb. The total number of nodes in a typical $(3+1)$-dimensional grid along a longitudinal and two transverse coordinates, as well as along the time variable, reaches $2048 \times 1024 \times 1024 \sim 10^9$ nodes. Analysis of the propagation of an array of complex numbers, representing the nonlinear evolution of a high-power ultrashort laser pulse on such a grid, along the longitudinal coordinate is, thus, equivalent to the analysis of an evolution of a few billion-dimensional problem within an interval covering $10^4$ steps in time.

Each step along the longitudinal coordinate involves about 20 operations of the forward and inverse fast Fourier transform (FFT). With the Cooley–Tukey algorithm properly optimized for our computational procedure, each FFT operation requires $M_q = 5N_q \log_2(N_q)$ operations with complex numbers. Here, $q$ is one of the transverse coordinates $\{x, y\}$ or the time variable $\eta$. The linear operator is computed through three forward and three inverse FFT operations. Computation of the nonlinear operator using the $k$th-order

Runge–Kutta method (in our computations, $k = 4, 5$) requires $42k$ FFT operations. Thus, the total number of floating-point operations needed to perform FFT on a grid including $N_z = 10{,}000$ steps along the longitudinal coordinate amounts to 100–200 PFlop (1 PFlop $= 10^{15}$ floating-point operations). The full number of operations required to implement a properly optimized computational algorithm, including auxiliary computational operations, operations needed to transfer, transpose, and copy the relevant data arrays, and technical procedures, is as large as 1000 PFlop.

The performance of a modern six-core Intel Core i7-4930K processor is 120 GFlops (1 GFlops $= 10^9$ floating-point operations per second). With such a processor, analysis of the evolution of a high-power ultrashort laser pulse in the multiple-filamentation regime with fixed parameters requires about a month of computing time.

Since the performance of conventional, even highest-speed, processors is insufficient, problems of this class are usually solved on computer clusters consisting of several hundred processor cores. As an important example, the performance of a 128-processor cluster of the Lomonosov supercomputer at Moscow State University is on the order of 1.3 TFlops (i.e., $1.3 \times 10^{12}$ floating-point operations per second). With such a computational speed, numerical analysis of the propagation of a high-power ultrashort laser pulse in the regime of multiple filamentation takes about a week. As shown below in Sections 4 – 7 of this paper, with GPU clusters a full numerical analysis of the propagation of a high-power ultrashort laser pulse in the regime of multiple filamentation can be performed on a laboratory computer station.

## 4. Exaflop computations on a laboratory computer station

In this work, numerical analysis of the nonlinear dynamics of high-power ultrashort laser pulses in the regime of multiple filamentation was performed on a laboratory computer station boosted with a cluster of Nvidia GeForce GTX 970 graphic accelerators. The performance of such GPU units can be as high as 2.3 TFlops. With proper optimization, such accelerators can perform exaflop computations within only a few days. Parallelizing program algorithms for GPU clusters is the key factor for the optimization of exaflop computations utilizing such video cards.

The scheme of parallel computations on a GPU cluster implemented in this work is sketched in Fig. 1b. In contrast to a standard method of parallel computations based on a message-passing interface (MPI) [27], our scheme employs a hybrid parallelizing technique, in which the computation of the nonlinear, dispersion, and diffraction operators is accelerated by combining an MPI interface with a compute unified device architecture (CUDA) [28]. The number of parallel MPI processes supported by the developed algorithm is determined by the number of video cards $M$ (for our laboratory computer station, $M = 4$). Each of these processes implements calculations using the split-step method (Fig. 1b). The two-dimensional Fourier transform is performed within the processor segment of the cluster using a standard library of programs. The dispersion, diffraction, and nonlinear operators in equation (1) are computed using the CUDA within the graphic segment of the cluster (Fig. 1b, c). To this end, the data are transferred from random access memory of the main processor to the GPU memory and back (Fig. 1b).

Figure 1c illustrates this computational procedure implemented on a grid consisting of $512 \times 512 \times 2048$ nodes on $x$-, $y$-, and $\eta$-axes, respectively. Colored $x\eta$-plane grid node layers are involved in parallel computations performed by one GPU. Computations performed by GPUs on each of these layers are organized in the units in accordance with the CUDA scheme. The total number of such units in our computational process amounts to 8192. Each unit, in turn, consists of 128 threads (Fig. 1c).

The GPU segment of the cluster computes the dispersion, diffraction, and nonlinear operators with such a high speed that the forward and inverse $x$-to-$y$ three-dimensional data-array transposition needed for two-dimensional FFT using the standard library of programs becomes the slowest process in the procedure.

When implemented on the platform of a four-core laboratory computer station with an Intel Core i5-4690 processor with an ASRock Z87 OC Formula motherboard and a graphic accelerator consisting of four 1164-core GeForce GTX 970 GPUs, our algorithm can accomplish a full spatio-temporal analysis of the dynamics of a high-power ultrashort laser pulse in the regime of multiple filamentation within one day. With such an organization of parallel computations, a specific-target-oriented optimization of parameters of laser pulses and a medium becomes realistic, greatly facilitating a search for the ranges of parameter space where unique physical regimes of the nonlinear dynamics of high-power ultrashort laser pulses are possible. In Sections 5–7, we present the results of exaflop computations performed on a laboratory computer station showing that ultrashort field waveforms with extremely short pulse widths can be generated as a result of complex spatio-temporal field transformations. Based on this analysis, we will define the parameter space within which nonlinear-optical phenomena can suppress the diffraction of single-cycle and subcycle field waveforms.

## 5. Dynamics of multiple filamentation

A typical picture of the spatio-temporal dynamics of an ultrashort laser pulse with a peak power $P$ two orders of magnitude higher than the self-focusing threshold $P_{cr}$ is displayed in Fig. 2. Here, calculations have been performed for ultrashort mid-infrared pulses with a central wavelength $\lambda = 3.9$ μm, input energy $W_0 = 270$ mJ, and input pulse width $\tau_0 = 100$ fs. High-peak-power femtosecond pulses at this wavelength are delivered by recently developed mid-infrared sources of generation based on optical parametric chirped-pulse amplification [29–32]. The dynamics of such pulses in the regime of multiple filamentation is of considerable interest as a way toward the generation of high-power single-cycle and subcycle pulses in the mid-infrared range, and in the context of interesting new phenomena that may be expected since the central wavelength of such pulses falls within the range of anomalous dispersion of many solid materials. A numerical analysis of single-filamentation dynamics [33, 34], which takes place for much lower ratios of the laser peak power to the critical power of self-focusing, suggests that unique propagation regimes, including formation of light bullets, may become possible for ultrashort laser pulses in the regime of anomalous dispersion.

A light beam with a peak power several orders of magnitude higher than the critical power of self-focusing ($P = 100P_{cr}$ for the propagation dynamics illustrated in

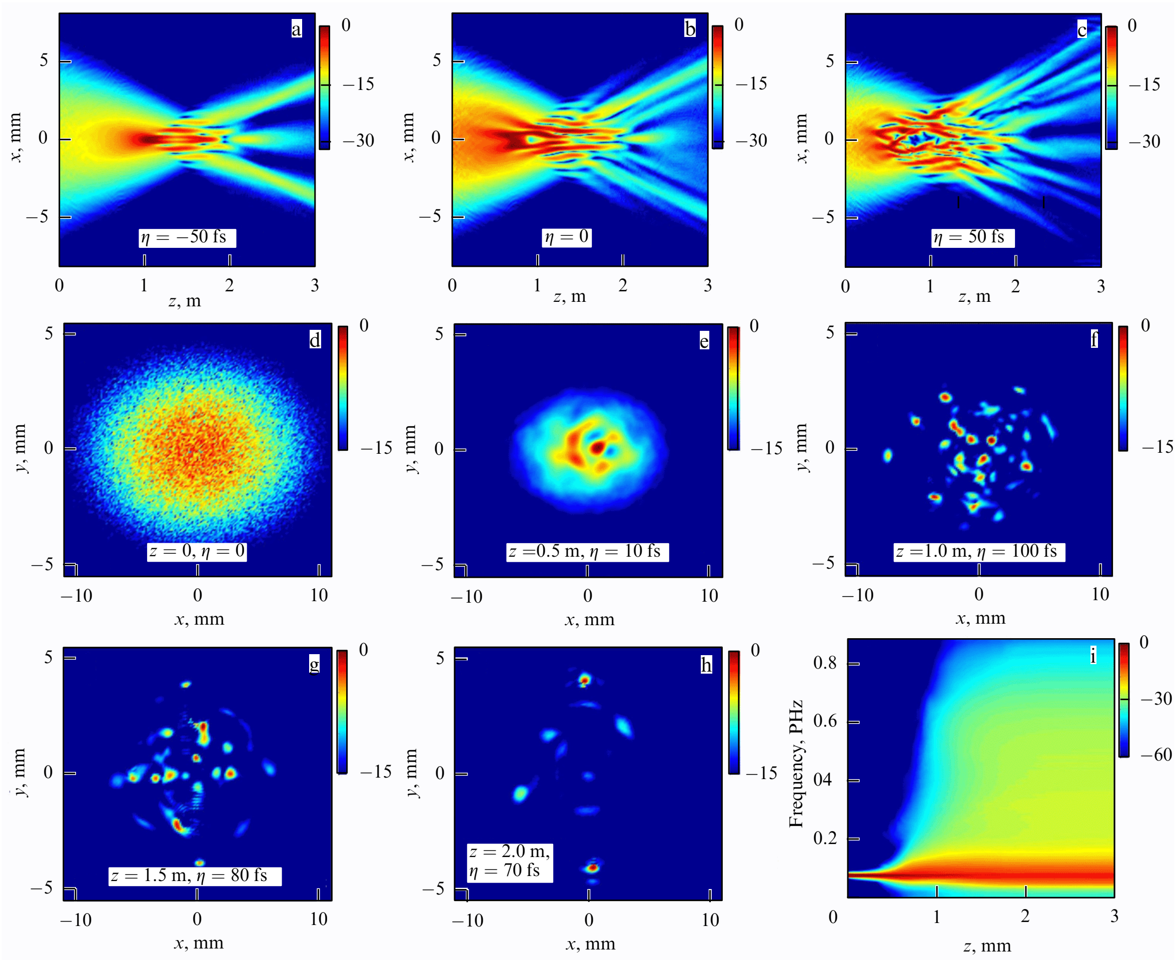


**Figure 2.** (Color online). Spatio-temporal dynamics of an ultrashort laser pulse with a central wavelength of 4 μm, a pulse width of 100 fs, and an energy of 270 mJ, propagating in a gas chamber filled with molecular nitrogen at a gas pressure of 4 atm: (a–c) spatial dynamics at the leading edge ($\eta = -50$ fs), (b) central part ($\eta = 0$), and (c) trailing edge ($\eta = 50$ fs) of the pulse; (d–h) transverse beam profiles at (d) $z = 0$ and $\eta = 0$, (e) $z = 0.5$ m and $\eta = 10$ fs, (f) $z = 1.0$ m and $\eta = 100$ fs, (g) $z = 1.5$ m and $\eta = 80$ fs, and (h) $z = 2.0$ m and $\eta = 70$ fs; (i) spatial evolution of the pulse spectrum integrated across the beam. The initial peak power of the laser pulse is $P = 100 P_{\rm cr}$. The beam is focused by a lens with focal length $f = 2$ m. Simulations were performed on four core processors and four 1664-core GeForce GTX 970 GPUs on a grid consisting of $2048 \times 512 \times 512 \times 12{,}000$ nodes on $\eta$-, $x$-, $y$-, and $z$-axes, respectively. The computational complexity of the problem reaches 1000 PFlop. The computing time is 4 days.

Fig. 2) exhibits complex temporal (Figs 2a–c), spatial (Figs 2d–h), and spectral (Fig. 2i) dynamics. The field structure turns out to be inhomogeneous across the beam and within the laser pulse, constantly changing as the beam propagates through the medium and displaying significant variations from the leading to the trailing edges of the pulse (Figs 2a–c). Such variations in the beam structure are due to a dynamic interplay between the Kerr and ionization nonlinearities, which changes from the leading edge of the pulse to its tail. The temporal structure of the field is, in turn, nonuniform across the beam.

A laser field with a peak power $P \gg P_{\rm cr}$ is unstable with respect to beam breakup into multiple filaments, seeded by random field intensity fluctuations within the light beam. The resulting spatial modulation instabilities give rise to field hot spots across the beam (Figs 2d, e) and eventually lead to a loss of coherence within the laser beam (Figs 2f–h). As a result of the joint action of the Kerr and ionization nonlinearities, the beam breaks up into multiple filaments (Figs 2b, c, f–h). This phenomenon is accompanied by efficient spectral broadening (Fig. 2i), which is typical of laser-induced filamentation and is often referred to as supercontinuum generation.

The high speed of computations provided by our parallelization algorithm and interactive feedback control over the modeling process, which becomes possible due to continual access to our laboratory computer cluster, enable a systematic detailed study of multiple filamentation by comparing the results of numerical simulations with estimates based on transparent physical models. As an important result, we emphasize that the typical length within which a laser beam breaks up into multiple filaments in numerical simulations agrees closely with the spatial modulation instability length as theoretically predicted by Bespalov and Talanov [20]. In numerical simulations presented in Fig. 2, multiple filamentation becomes noticeable within a typical propagation length $l_{\rm m}$ on the order of 1 m (Fig. 2f). In the Bespalov–Talanov theory [20], on the other hand, the typical length within which spatial modulation instabilities tend to build up is on the order of the nonlinear length, $l_{\rm nl} = c(\omega n_2 I_0)^{-1}$, where $I_0$ is the field intensity. For the propagation regime illustrated in Fig. 2, where $I_0 \approx$ 20 TW cm$^{-2}$ and $n_2 = 1.4 \times 10^{-7}$ cm$^2$ TW$^{-1}$, the buildup of modulation instabilities closely follows the $\exp(z/l_{\rm nl})$ growth rate predicted by the Bespalov–Talanov theory. In this

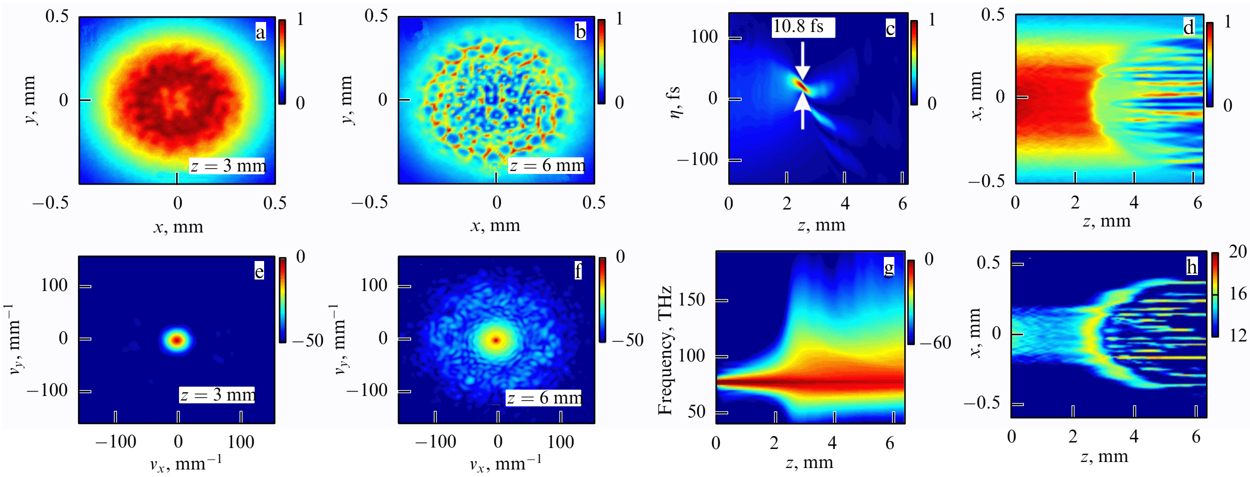


**Figure 3.** (Color online.) Multiple filamentation of a high-peak-power laser beam for a laser pulse with a central wavelength of 3.9 μm, an initial pulse width of 200 fs, an energy of 3.1 mJ, and an initial beam diameter of 1.25 mm propagating in a YAG plate: (a, b) transverse beam profiles at the point of maximum pulse compression, (a) $z = 3.0$ mm and (b) $z = 6.0$ mm; (c) temporal evolution on the beam axis; (d) beam dynamics; (e, f) beam angular spectrum at the point of maximum pulse compression, (e) $z = 3.0$ mm and (f) $z = 6.0$ mm; (g) spatial evolution of the spectrum integrated over the beam cross section; (h) beam dynamics at the trailing edge of the pulse. The initial peak power of the laser pulse is $P = 480P_{\rm cr}$.

regime, for beam instabilities seeded by noise intensity fluctuations, a gain of 100 is achieved within a propagation length of about 1 m. Within a broad range of input laser beam parameters, the length within which multiple filamentation was observed in numerical simulations agrees well with the predictions of the Bespalov–Talanov theory for the modulation instability buildup length. This finding allows strongly coupled complex processes involved in nonlinear spatio-temporal field dynamics and observed in numerical simulations to be interpreted in a clear, physically transparent way.

## 6. Self-compression of high-peak-power light pulses

Soliton self-compression of laser pulses in the anomalous dispersion regime is widely used for the generation of ultrashort light pulses in optical fibers [35, 36]. The spatio-temporal $(3+1)$-dimensional dynamics of freely propagating laser beams with a peak power well above the critical power of self-focusing is, however, much more complicated than the dynamics of light pulses in optical fibers, which can be accurately described within the framework of the thoroughly developed model of the generalized nonlinear Schrödinger equation with one temporal and one spatial coordinate [35]. As shown in Section 5, the spatio-temporal evolution of optical fields with peak powers $P \gg P_{\rm cr}$ in the regime of anomalous dispersion can often involve beam breakup into multiple filaments, leading to the loss of beam connectedness and, eventually, spatial coherence (Fig. 3). Remarkably, despite all the complexity of their spatio-temporal dynamics, efficient self-compression of high-peak-power ultrashort light pulses is still possible, as illustrated in Fig. 3, without the loss of field connectedness and spatial coherence through beam breakup into multiple filaments.

Of key significance for this regime of nonlinear dynamics is that the typical lengths of self-compression and modulation instability, $l_{\rm c}$ and $l_{\rm m}$, should obey the inequality $l_{\rm c} < l_{\rm m}$. When this condition is satisfied, a light pulse experiences self-compression to its minimum pulse width, as a result of the joint action of anomalous dispersion and nonlinearity, before the beam breaks up into multiple filaments. As can be seen from simulations presented in Fig. 3, on the propagation length $z \approx l_{\rm c} \approx 2.4$ mm, self-compression yields a subcycle field waveform with a pulse width of about 10.8 fs (Fig. 3c). Within this propagation length, the beam still does not lose its connectedness (Fig. 3d), with its angular spectrum (Fig. 3e) showing virtually no features that would be indicative of the developed spatial modulation instabilities.

Within longer propagation paths ($z > l_{\rm m} \approx 3$ mm), modulation instabilities become noticeable (Figs 3a, b, d, f, h), with field hot spots appearing across the beam (Figs 3a, b). The angular spectrum corresponding to this phase of the beam dynamics displays noticeable distortions, indicating off-axial field components (Fig. 3f). Beam breakup due to modulation instability is accompanied by multiple filamentation (Figs 3d, h), caused by the joint action of the Kerr and ionization nonlinearities.

Thus, our numerical simulations confirm that, when the spatial length of self-compression is kept shorter than the length required for the build-up of modulation instabilities, $l_{\rm c} < l_{\rm m}$, high-peak-power light pulses can undergo efficient self-compression without the loss of beam spatial coherence. This effect is of key significance for identifying the physical scenarios whereby single-cycle and subcycle light bullets can be generated in the regime of anomalous dispersion. This phenomenon is discussed below in Section 7.

## 7. Subcycle light bullets

Single-cycle and subcycle light pulses, which have become available due to new approaches to laser technologies [37–40], provide a unique tool for studying ultrafast processes in matter [41]. Identifying paths toward higher intensities in such pulses and higher efficiencies of their generation is one of the key challenges in ultrafast optical physics. The analysis presented below in this section outlines one of the promising approaches to confront these challenges.

Laser-induced filamentation is widely applied for the compression of high-intensity light pulses at the level of peak power $P \sim (3-10)P_{\rm cr}$. Scaling this pulse-compression

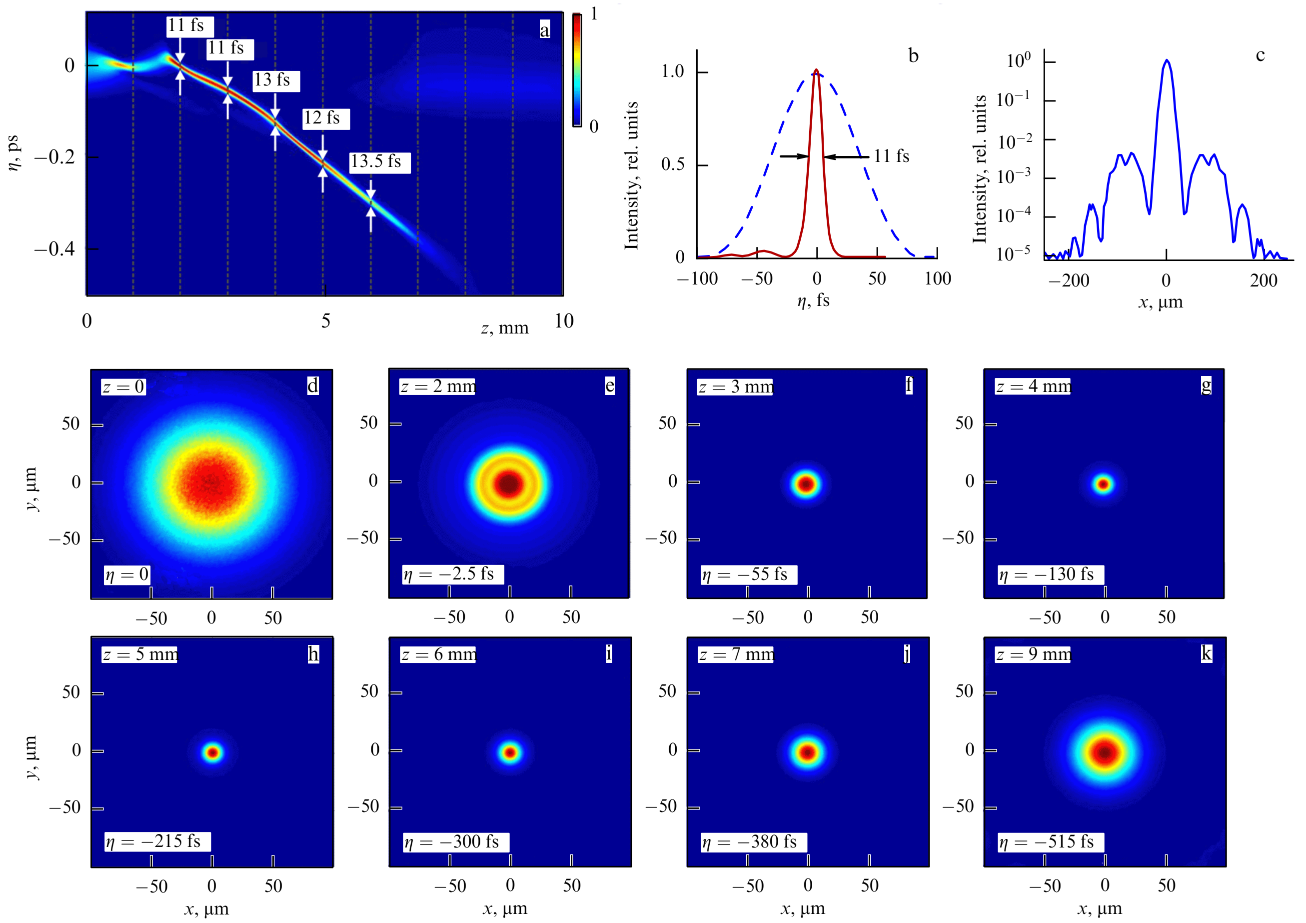


**Figure 4.** (Color online.) Generation of light bullets as a part of the evolution of a laser pulse with a central wavelength of 3.9 μm, an initial pulse width of 80 fs, an energy of 40 μJ, and an initial beam diameter of 140 μm propagating in a YAG plate: (a) temporal evolution on the beam axis; (b) temporal evolution of the pulse on the beam axis at $z = 3$ mm; (c) one-dimensional cut of the transverse beam profile at $\eta = 0$, $y = 0$, and $z = 3$ mm; (d–k) transverse beam profiles at (d) $z = 0$ and $\eta = 0$, (e) $z = 2$ mm and $\eta = -2.5$ fs, (f) $z = 3$ mm and $\eta = -55$ fs, (g) $z = 4$ mm and $\eta = -130$ fs, (h) $z = 5$ mm and $\eta = -215$ fs, (i) $z = 6$ mm and $\eta = -300$ fs, (j) $z = 7$ mm and $\eta = -380$ fs, and (k) $z = 9$ mm and $\eta = -515$ fs.

technology to higher peak powers, however, faces serious difficulties. The breakup of a high-peak-power laser beam into multiple filaments (see Section 5), leading to a loss of beam connectedness and, eventually, spatial coherence [42], is one such problem, making power scaling of filamentation-assisted pulse compression difficult. A series of numerical simulations performed on our laboratory computer station enhanced with a cluster of graphic accelerators helps identify approaches whereby this problem can be addressed. Our numerical simulations show that self-compression of light pulses with peak powers $P \gg P_{\rm cr}$ in the regime of anomalous dispersion enables the generation of high-peak-power subcycle light pulses without the loss of spatial coherence. Moreover, the results of these simulations, presented below in this section, demonstrate that high-peak-power single-cycle and subcycle light pulses can be produced in this regime in the form of light bullets, where field localization in time is combined with spatial beam confinement. This becomes possible due to a delicate balance between dispersion and nonlinearity with simultaneous suppression of diffraction-induced beam divergence by the Kerr lens, acting jointly with the ionization nonlinearity.

With numerous simplifying assumptions regarding the properties of dispersion and optical nonlinearity of a medium, as well as concerning the symmetry and dimensionality of a light beam, criteria necessary for the existence of light bullets can be formulated as closed-form semianalytical expressions [43, 44]. However, physical scenarios enabling the generation of extremely short, single-cycle and subcycle light bullets can only be identified through an adequate revision of models toward including realistic dispersion profiles, higher order optical nonlinearities, ultrafast ionization, and beams without axial symmetry. Numerical analysis of such pulse evolution scenarios is a complex computational problem, requiring exaflop computations. Still, as the simulations presented in Fig. 4 show, this problem can be solved through properly optimized computations on a laboratory computer station enhanced with a cluster of graphic accelerators.

In Fig. 4, we present the results of numerical simulations performed for a light pulse with an initial pulse width of 80 fs, a central wavelength of 3.9 μm, an energy of 40 μJ, and an initial beam diameter of 140 μm propagating in the region of anomalous dispersion in an yttrium aluminum garnet (YAG) crystal. At the initial stage of spatio-temporal field dynamics, self-focusing is seen to radically decrease the beam diameter. As can be seen in Figs 4d–f, within a propagation length of a few millimeters, the beam diameter decreases to a few micrometers. However, within the next stages of field evolution (3–7 mm), the beam diameter remains virtually unchanged (Figs 4f–j) even though, in the linear regime, its drastic decrease within the initial stage of beam dynamics would have resulted in a significant enhancement of diffraction-induced beam divergence.

Beam self-focusing at the initial stage of field evolution (up to $z \approx 2$ mm in Fig. 4a) is accompanied by temporal self-compression as a result of the joint action of anomalous dispersion and optical nonlinearity. At a distance $z \approx 2$ mm, the pulse width decreases to about 11 fs (Figs 4a, b). As the field waveform propagates further along the medium (3–7 mm in Fig. 4a), its pulse width remains virtually unchanged. On the entire propagation length (from 2 to 7 mm in Fig. 4a), the pulse width of the optical field waveform never exceeds the field cycle (13 fs) of 3.9-μm radiation. Notably, such propagation dynamics would not have been possible in the linear regime, where material dispersion would have stretched the pulse within a typical propagation length of only 50 μm.

Our numerical analysis reveals that spatially and temporally localized field propagation becomes possible within the studied parameter space due to a photon bath in the beam periphery (seen as a pedestal in Fig. 4c), which provides a constant energy supply to the central part of the beam. Temporal field dynamics under these conditions, in some approximation, follows a solitonic pulse evolution (viz., soliton pulse self-compression [35]) only on a propagation length $z \approx 1$ mm. Further on along the beam path, the field propagates in the form of a light bullet, sustained by strongly coupled spatial and temporal self-action effects. In this regime, light bullets cannot be adequately described in terms of spatial or temporal solitonic phenomena.

The light bullet shown in Fig. 4 sustains a pulse width of 11–13 fs within its entire evolution path (Fig. 4a) and contains up to 15% of the input pulse energy (at $z \approx 3$ mm). The temporal envelope of the overall field waveform containing this light bullet features a central peak acquiring up to 50% of the total pulse energy against an extended pedestal (Fig. 4b). This pedestal plays the role of the photon bath confining the field to a short time interval.

An appropriate choice of initial parameters is of key significance for the generation of single-cycle and subcycle light bullets. As can be seen from the results presented in Fig. 4a, subcycle pulses are formed within the initial stage of field evolution ($z < 1$ mm), where solitonic effects play the dominant role. This field dynamics can be scaled within the relevant parameter space using the physically transparent scaling laws of soliton self-compression. This finding makes it much easier to identify the parameter range for the generation of high-power subcycle light bullets. The subsequent spatio-temporal field dynamics leading to light bullet formation do not allow an equally physically intuitive analysis to be made in terms of solitonic dynamics. The optimal range of parameters for the generation of such light bullets can then only be defined through a detailed numerical analysis performed for specific properties of a laser source used to deliver the input short-pulse optical field. The methods of physical and numerical analysis presented in this paper open new avenues for solving such problems.

## 8. Conclusion

Methods of physical modeling and numerical analysis highlighted in this paper are instrumental in solving a broad class of computationally complex physical problems involving the intricate spatio-temporal dynamics of ultrashort light pulses with a peak power well above the critical power of self-focusing.

Exaflop computations performed with the application of these methods on a laboratory computer station with a cluster of graphic processing units reveal new unique phenomena of the spatio-temporal dynamics of superpower ultrashort laser pulses. We have demonstrated that unprecedentedly short light bullets can be generated as a part of these dynamics, providing optical field localization both in space and time through a balance between dispersion and nonlinearity with simultaneous suppression of diffraction-induced beam divergence due to the joint effect of Kerr and ionization nonlinearities. Methods of physical and numerical analysis presented in this paper enabled handling computationally complex simulations for a target-specific optimization of parameters of laser pulses and properties of nonlinear media for the implementation of unique physical scenarios in the nonlinear dynamics of high-power ultrashort light pulses.

**Acknowledgments**
This research was partially supported by the Russian Foundation for Basic Research (project Nos 14-29-07182, 16-02-00843, 15-32-20897, and 14-22-02105) and the Welch Foundation (grant No. A-1801). Research into the nonlinear optics of ultrashort pulses in the mid-infrared range was supported by the Russian Science Foundation (project No. 14-12-00772).

## References

1. Fattahi H et al. *Optica* **1** 45 (2014)
2. Korzhimanov A V et al. *Phys. Usp.* **54** 9 (2011); *Usp. Fiz. Nauk* **181** 9 (2011)
3. Couairon A, Mysyrowicz A *Phys. Rep.* **441** 47 (2007)
4. Bergé L et al. *Rep. Prog. Phys.* **70** 1633 (2007)
5. Serebryannikov E E, Goulielmakis E, Zheltikov A M *New J. Phys.* **10** 093001 (2008)
6. Chin S L *Femtosecond Laser Filamentation* (Springer Series on Atomic, Optical, and Plasma Physics, Vol. 55) (New York: Springer, 2010)
7. Chekalin S V, Kandidov V P *Phys. Usp.* **56** 123 (2013); *Usp. Fiz. Nauk* **183** 133 (2013)
8. Zheltikov A *Appl. Phys. B* **77** 143 (2003)
9. Kasparian J et al. *Science* **301** 61 (2003)
10. Zheltikov A M *Phys. Usp.* **49** 605 (2006); *Usp. Fiz. Nauk* **176** 623 (2006)
11. Silva F et al. *Nature Commun.* **3** 807 (2012)
12. Lanin A A et al. *Opt. Lett.* **39** 6430 (2014)
13. Liang H et al. *Opt. Lett.* **40** 1069 (2015)
14. Hauri C P et al. *Appl. Phys. B* **79** 673 (2004)
15. Couairon A et al. *Opt. Lett.* **30** 2657 (2005)
16. Skupin S et al. *Phys. Rev. E* **74** 056604 (2006)
17. Kartashov D et al. *Phys. Rev. A* **86** 033831 (2012)
18. Malevich P N et al. *Opt. Express* **20** 18784 (2012)
19. Malevich P N et al. *Opt. Lett.* **40** 2469 (2015)
20. Bespalov V I, Talanov V I *JETP Lett.* **3** 307 (1966); *Pis'ma Zh. Eksp. Teor. Fiz.* **3** 471 (1966)
21. Voronin A A et al. *Opt. Commun.* **291** 299 (2013)
22. Voronin A A, Zheltikov A M *Phys. Rev. A* **94** 023824 (2016)
23. Voronin A A, Zheltikov A M *Phys. Rev. A* **90** 043807 (2014)
24. Zhokhov P A, Zheltikov A M *Phys. Rev. Lett.* **110** 183903 (2013)
25. Keldysh L V *Sov. Phys. JETP* **20** 1307 (1965); *Zh. Eksp. Teor. Fiz.* **47** 1945 (1964)
26. Popov V S *Phys. Usp.* **47** 855 (2004); *Usp. Fiz. Nauk* **174** 921 (2004)
27. Foster I T *Designing and Building Parallel Programs: Concepts and Tools for Parallel Software Engineering* (Reading, Mass.: Addison-Wesley, 1995)
28. Manavski S A, Valle G *BMC Bioinform.* **9** S10 (2008)
29. Popmintchev T et al. *Science* **336** 1287 (2012)

30. Mitrofanov A V et al. *Sci. Rep.* **5** 8368 (2015)
31. Mitrofanov A V et al. *Phys. Usp.* **58** 89 (2015); *Usp. Fiz. Nauk* **185** 97 (2015)
32. Mitrofanov A V et al. *Opt. Lett.* **40** 2068 (2015)
33. Durand M et al. *Phys. Rev. Lett.* **110** 115003 (2013)
34. Majus D et al. *Phys. Rev. Lett.* **112** 193901 (2014)
35. Agrawal G P *Applications of Nonlinear Fiber Optics* (San Diego: Academic Press, 2001)
36. Zheltikov A M *Phys. Usp.* **50** 705 (2007); *Usp. Fiz. Nauk* **177** 737 (2007)
37. Goulielmakis E et al. *Science* **317** 769 (2007)
38. Wirth A et al. *Science* **334** 195 (2011)
39. Huang S-W et al. *Nature Photon.* **5** 475 (2011)
40. Balciunas T et al. *Nature Commun.* **6** 6117 (2015)
41. Corkum P B, Krausz F *Nature Phys.* **3** 381 (2007)
42. Zheltikov A M *Phys. Rev. A* **88** 063847 (2013)
43. Silberberg Y *Opt. Lett.* **15** 1282 (1990)
44. Moll K D, Gaeta A L, Fibich G *Phys. Rev. Lett.* **90** 203902 (2003)